



HAL
open science

Bio-Sourced Zeolite-Templated Carbons for the Development of Efficient ORR Catalysts

Daniele Oliveira, Thibaud Aumond, Lola Louprias, Leonardo Santos, Vinícius Caldeira, Christine Canaff, Sibeles Pergher, Aurélien Habrioux, Alexander Sachse

► **To cite this version:**

Daniele Oliveira, Thibaud Aumond, Lola Louprias, Leonardo Santos, Vinícius Caldeira, et al.. Bio-Sourced Zeolite-Templated Carbons for the Development of Efficient ORR Catalysts. *ChemCatChem*, 2023, 15 (12), pp.e202201494. 10.1002/cctc.202201494 . hal-04102097

HAL Id: hal-04102097

<https://hal.science/hal-04102097>

Submitted on 22 May 2023

HAL is a multi-disciplinary open access archive for the deposit and dissemination of scientific research documents, whether they are published or not. The documents may come from teaching and research institutions in France or abroad, or from public or private research centers.

L'archive ouverte pluridisciplinaire **HAL**, est destinée au dépôt et à la diffusion de documents scientifiques de niveau recherche, publiés ou non, émanant des établissements d'enseignement et de recherche français ou étrangers, des laboratoires publics ou privés.

Bio-sourced zeolite-templated carbons for the development of efficient ORR catalysts

Daniele S. Oliveira,^[a,b] Thibaud Aumond,^[a] Lola Loupias,^[a] Leonardo L. Santos,^[a,b] Vinícius P. S. Caldeira,^[c] Christine Canaff,^[a] Sibebe B. C. Pergher,^[b] Aurélien Habrioux^{*[a]} and Alexander Sachse^{*[a]}

[a] Dr. D. S. Oliveira, Dr. T. Aumond, Dr. L. Loupias, Dr. L. L. Santos, C. Canaff, Dr. A. Habrioux, Dr. A. Sachse
Université de Poitiers, Institut de Chimie des Milieux et Matériaux de Poitiers (IC2MP) - UMR 7285 CNRS, UFR SFA, Bât. B27, 4 rue Michel Brunet, TSA
51106, 86073 Poitiers Cedex 9 – France.

E-mail: alexander.sachse@univ-poitiers.fr, aurelien.habrioux@univ-poitiers.fr

[b] Dr. D. S. Oliveira, Dr. L. L. Santos, Dr. S. B. C. Pergher
Molecular Sieves laboratory (LABPEMOL), Chemistry Institute, University of Rio Grande do Norte, Av Senador Salgado Filho, 3000, CEP : 59078-970,
Natal – RN, Brazil.

[c] Dr. V. P. S. Caldeira
Laboratory of Catalysis, Environment and Materials (LACAM), Department of Chemistry, State University of Rio Grande do Norte, 59610-210, Mossoró –
RN, Brazil.

Abstract: Bio-sourced Zeolite-Templated Carbons (ZTCs) were achieved through the use of glycerol as carbon source. A systematic study of the textural and chemical properties is presented on ZTCs achieved at synthesis temperatures between 300 °C and 800 °C. Textural properties are importantly impacted through increasing synthesis temperature. ZTCs featuring high textural quality were synthesized at temperatures as low as 400 °C. Oxygen content was further found to be importantly impacted by the synthesis temperature. This latter plays a crucial role when materials are functionalized with thiourea, as high oxygen content allows for maximizing the incorporation of N and S in the ZTC. Functionalized bio-sourced ZTCs allowed for achieving unparalleled ORR activities and hydroxyl selectivities when compared to other functionalized carbon materials such as graphene-based catalysts.

Introduction

The production of bio-derived glycerol has been steadily growing over the past 20 years and production exceeds currently global demand by a factor of six.^[1] This explains the quest for sound glycerol valorization strategies. Numerous approaches aim at the conversion of glycerol for the production of added-value chemicals and fuels. Catalytic strategies based on steam reforming, aqueous phase reforming, dry reforming, hydrogenolysis and selective oxidation are largely covered topics in the scientific literature.^[2]

The development of biomass-derived carbon materials is currently one of the hot topics in advanced materials design.^[3] The use of lignocellulose-derived precursors^[4] or tannins^[5] is widely studied for the production of sustainable materials with defined textural properties. The transformation of glycerol into added-value materials has only scarcely been reported. A limited number of reports present the development of activated carbons from glycerol.^[6-8] Gonçalves *et al.*^[9] recently reported the use of crude glycerol for the synthesis of activated carbons, which proved promising for the development of bio-derived supercapacitor electrodes.

Activated carbons yet feature highly disordered structures of cross-linked, randomly packed graphene sub-units and hence

present unstructured porous topologies.^[10] Since the beginning of the current century a new class of carbon materials was disclosed and named Zeolite-Templated Carbons (ZTCs).^[11] The first synthesis of high quality ZTC was described using a two-step method in which the zeolite is firstly impregnated with polymer, and secondly followed by chemical vapor deposition of a gas.^[12] Later, a one-step method was described allowing the formation of high-quality ZTC through the use of ethylene or acetylene, which diffuse and polymerize within the microporous network of a sacrificial zeolite.^[13,14] After carbon formation within the zeolite the template is dissolved and the ZTC is recovered. ZTCs are a negative copy of the zeolite texture and hence feature tailored porous topologies. They have been described as 3D graphenes.^[15] The combination of excellent electrical conductivity and unparalleled textural properties makes ZTCs very promising for the design of energy conversion and storage devices.^[16-20]

The use of alternative carbon sources for the synthesis of ZTCs was recently proposed.^[21, 22] Oxygen containing hydrocarbons, such as methanol, ethanol, isopropanol, acetone, tetrahydrofuran, and diisopropyl ether were tested in the synthesis of ZTCs by Ryoo and co-workers.^[23] The authors found that these lead to the generation of olefins at the applied synthesis condition, *i.e.* 650-700 °C. It is these olefins that then react within the zeolite microporosity and allow for the formation of the carbon skeleton.

In the present contribution we firstly study the synthesis of bio-sourced ZTCs from glycerol synthesized in the temperature range from 300 to 800 °C. The use of glycerol permits the synthesis of structured ZTCs even at temperatures as low as 400 °C. The thorough characterization of the hybrids (zeolite/carbon) and pure carbons allowed to assess that the synthesis temperature importantly impacts textural and chemical properties. After functionalization with thiourea the bio-sourced ZTCs allow for conspicuous ORR activities.

Results and Discussion

Characterization of the hybrid materials

The structural packing density (SPD) gives the amount of carbonaceous material per unit of zeolite mass and can be calculated from the TGA mass loss curves of the hybrid materials. The SPD increases from 0.16 to almost 0.32 $\text{g}_\text{C} \text{g}_\text{Z}^{-1}$ for the hybrids achieved at 300 and 500 °C, respectively (**Figure 1a**). This suggests that at 300 °C the zeolite is only partially filled with carbonaceous compounds. Values of SPDs from 0.30 to 0.34 $\text{g}_\text{C} \text{g}_\text{Z}^{-1}$ are typically observed for hybrid materials leading to high quality ZTCs achieved from ethylene in **FAU** structured zeolites.^[24] With increasing synthesis temperature the SPD slightly decreases to reach 0.27 $\text{g}_\text{C} \text{g}_\text{Z}^{-1}$ at 800 °C. It is further to note that the mean temperature of combustion is impacted by the synthesis temperature (**Figure 1b**). From 300 to 500 °C the mean temperature of combustion decreases slightly from 540 to 532 °C, respectively. This value increases thereafter importantly and reaches 565 °C for the material achieved at 800 °C. This variation in the value for the mean combustion temperature indicates that the carbon synthesized at higher temperatures presents a higher degree of condensation of the carbonaceous species in the zeolite channels.^[25]

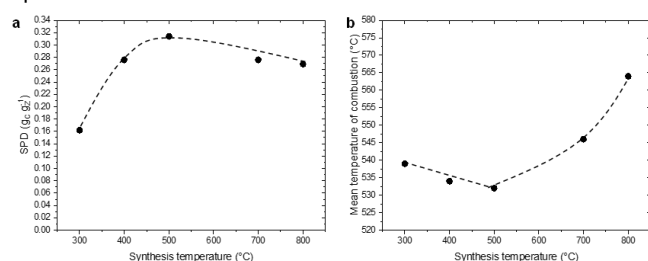
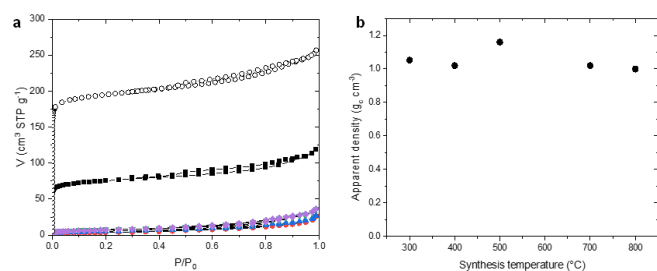


Figure 1. Evolution of SPD (a) and mean temperature of combustion (b) as a function of the synthesis temperature.

From the nitrogen physisorption isotherms at 77 K it is possible to observe that only the hybrid achieved at 300 °C presents incomplete zeolite micropore obstruction (**Figure 2a**). The sample features a remaining micropore volume of 0.10 $\text{cm}^3 \text{g}^{-1}$, hence 62% of the zeolite micropore volume is blocked. For hybrids achieved above 400 °C the entirety of the micropore volume is inaccessible to nitrogen. It is interesting to note that



hybrid

Figure 2. Nitrogen physisorption isotherms at 77 K (a) and apparent density as a function of the synthesis temperature (b). Color code: template USY zeolite (black hollow symbols), 300 °C (black symbols), 400 °C (red symbols), 500 °C (blue symbols), 700 °C (green symbols) and 800 °C (purple symbols).

materials present, independently of the synthesis temperature, a similar apparent density of the carbonaceous phase between 1

and 1.1 $\text{g}_\text{C} \text{cm}^{-3}$ (**Figure 2b**). This finding indicates similar topology of the carbonaceous species forming within the zeolite micropores.

Characterization of the carbon materials

From the nitrogen physisorption isotherm of the ZTC-300 sample it is interesting to observe that the desorption branch does not loop the adsorption branch at the relative pressure of 0.43 (**Figure 3a**). This is classically observed for not fully cross-linked polymers and can be ascribed to deformation/swelling of the network during adsorption.^[26] This hence indicates that the carbon skeleton is not fully condensed at 300 °C. For higher synthesis temperatures this phenomenon is much reduced, suggesting that the carbon skeleton presents higher rigidity.

The micropore volume is lowest for the ZTC-300 material (0.65 $\text{cm}^3 \text{g}^{-1}$) (**Figure 3b, Table S1**). Likewise this sample does not allow for observing any peaks in the XRD powder pattern, indicating that no structural long-range order is present in this sample (**Figure 3c**). For carbons achieved at 400 °C (ZTC-400 sample) and above the

micropore volume amounts to approximately 1 $\text{cm}^3 \text{g}^{-1}$ and for all the samples a characteristic XRD peak at approximately 6.5° 2θ can be observed which corresponds to the channel-to-channel structure of the zeolite template.^[27] The position of the peak shifts from 7.0° at 400 °C to 6.4° 2θ at 700 and 800 °C, indicating expansion of the pore-to-pore distance in the ZTC with increasing synthesis temperature. Similar can be inferred from the NLDFT pore size distribution (**Figure S5**).

The absence of a peak at approximately 25° 2θ, in the XRD patterns indicates the absence of extra ZTC carbon on the external surface. This confirms the good quality of the ZTCs obtained using glycerol as carbon source.

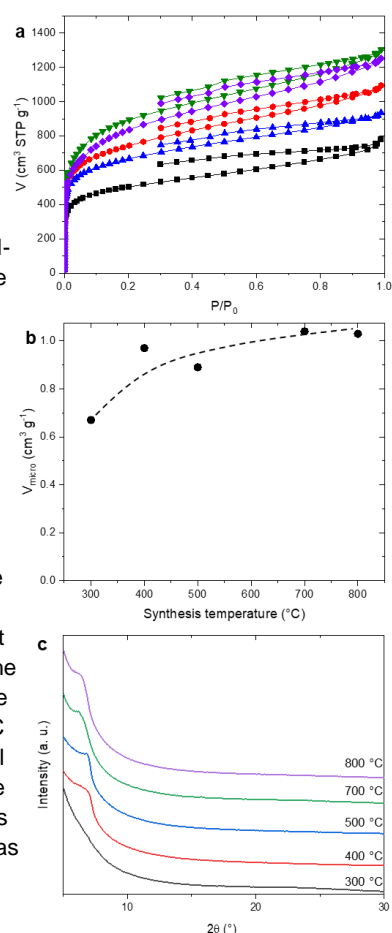


Figure 3. Nitrogen physisorption isotherms at 77 K (a). Evolution of the micropore volume as a function of the synthesis time (b). X-ray diffraction patterns of materials achieved at different temperature (c). Color code: 300 °C (black), 400 °C (red), 500 °C (blue), 700 °C (green) and 800 °C (purple).

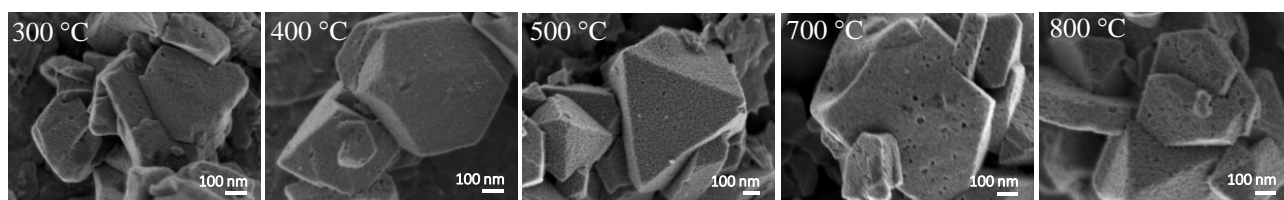
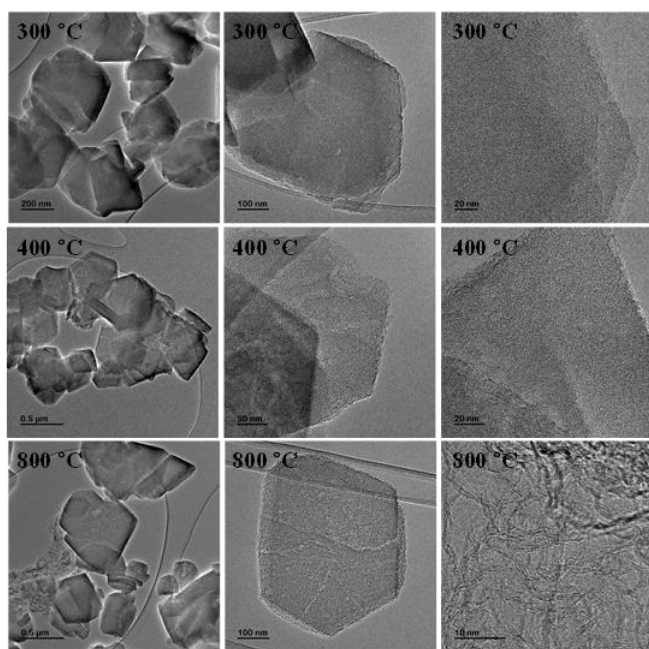


Figure 4. SEM images of ZTCs achieved at different synthesis temperatures.

The SEM images allow to observe that for all synthesis times replicas of the zeolite morphology are achieved. By closer observing the sample achieved at 300 °C one can note that the edges of the particles are smoother than for samples synthesized at higher temperatures (**Figure 4**). Further insights on the texture were achieved from TEM, which allows for the observation of individual particles that present similar textural properties compared to the template zeolite (**Figure 5**). For the sample achieved at 300 °C (ZTC-300) unstructured microporosity can be observed. It is further interesting to note the absence of mesoporosity for this sample. The low SPD and the incomplete filling of the zeolite microporosity suggest that these mesopores are probably lost during the zeolite dissolution process by the reaction of radical polyaromatic species.^[25] This hence indicates that the carbon species developing at 300 °C rather consist of smaller, uncondensed polyaromatic hydrocarbons. The TEM images of the ZTC-400 sample present the morphological features of the zeolite and the transcription of steamed mesopores. The high resolution TEM image of this sample allows for observing long-range structured microporosity. The TEM image of the ZTC-800 material allows to observe next to the carbon particles resulting from the zeolite templating the presence of turbostratic carbon.^[28] This high temperature synthesis hence leads to the presence of extra-ZTC carbon



species.

Figure 5. TEM images of ZTC-300 (scale bars from right to left: 200, 100 and 20 nm), ZTC-400 (scale bars from right to left: 500, 50 and 20 nm) and ZTC-800 (scale bars from right to left: 500, 100 and 10 nm).

The zeolite dissolution allows to remove the entirety of inorganic species from the carbon compounds. The TGA curves present complete weight loss, indicating full oxidation of the carbonaceous species extracted from the hybrid materials

(**Figure S4**). The mean temperature of combustion presents a similar tendency as for the hybrid materials. Its value is minimal for ZTC-500 and maximal for ZTC-800 and amounts to 515 and 558 °C, respectively (**Figure 6**). This suggests that the carbons achieved at temperature below 500 °C present a higher oxygen content, whilst carbons prepared at higher temperatures present a higher degree of condensed aromatic cycles.^[29]

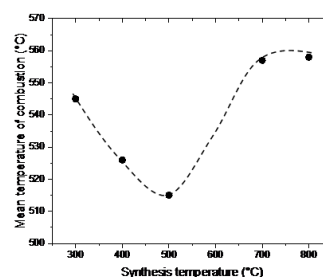


Figure 6. Mean temperature of combustion of ZTCs synthesized at different temperatures.

In the synthesis of ZTCs using glycerol as carbon precursor, glycerol was directly injected to the reactor at the target temperature. Hence, transformation of glycerol as a function of the temperature probably occurs. Dou *et al.*^[30] studied the thermal degradation of glycerol under nitrogen atmosphere by TGA. Complete degradation was observed for pure glycerol in a temperature range of 130 to 250 °C. The authors studied the composition of the degradation products by FTIR and reported the presence of compounds containing C=C and C=O bonds next to H₂O, CO₂ and CH₄ in the outflow. The pyrolysis of glycerol in the range of 650 to 700 °C has been described by Dalai and co-workers.^[31] The authors detected the presence of essentially CO, H₂, CO₂, CH₄ and C₂H₄. It can hence be assumed that degradation products presenting olefinic and carbonylic functions constitute the precursor mixture of the carbons achieved at temperature below 400 °C. At higher syntheses temperatures (500 °C and above) it can be assumed that the carbons are majorly formed from ethylene. This is confirmed by the C/H and the C/O ratios of the carbons (**Figure 7**). Indeed, the C/O ratio increases from 9 to 17 for ZTC-300 and ZTC-800. The materials achieved at lower synthesis temperatures present thus a higher degree of oxygenated carbon. The C/H ratios only little evolve as a function of the synthesis temperature from 3.0 to 4.5, indicating a higher degree of condensed carbon skeleton with increasing temperature.

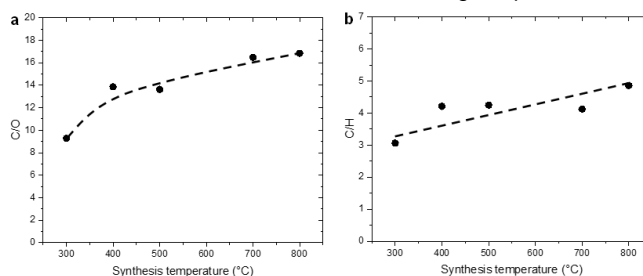


Figure 7. Atomic C/O (a) and C/H ratio (b) of ZTCs as a function of the synthesis temperature.

To further investigate the chemical nature of the samples Raman spectra were recorded at 532 nm (**Figure 8a**). Three features can be distinguished in the Raman shift range between 1100 and 1700 cm^{-1} and are ascribed to the G, D and S bands. The G band can be related to the vibrational modes associated with the asymmetric stretching of all sp^2 carbon atoms in the sample, while the D band is attributed to the breathing mode in aromatic rings.^[32-34] The G band is centered at 1600 cm^{-1} for all samples, which is a typical value for large polyaromatic hydrocarbons or nanocrystalline graphite.^[35] It is interesting to note that the D band position is impacted by the synthesis temperature and red-shifts for materials achieved with increasing temperature (**Figure 8b**). This suggests that the cluster size of polyaromatic entities increases with increasing temperature,^[36] which might hint the presence of sp^3 carbons in samples achieved at lower temperatures. The apparition of the S band in all of the samples is related to the topology of the carbon species that can develop in zeolite pores and are composed of elongated polyaromatic units, and is typically observed in rylene-type molecules or carbon nanoribbons.^[16,28] The intensity ratio of the D and G bands increases slightly with increasing synthesis temperature, indicating a higher degree of edges in carbons achieved at higher temperatures (**Figure 8c**). A similar tendency is observed for the intensity ratio of S and G bands, which suggests a higher amount of condensed aromatic units with pseudo one-dimensional D_{2h} point symmetry.^[37]

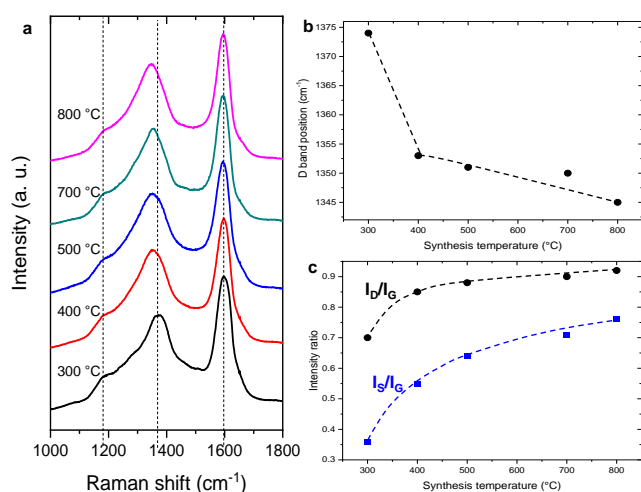


Figure 8. Raman spectra of materials synthesized at different synthesis temperatures (a). Raman D band position (b) and I_D/I_G and I_S/I_G intensity ratios as a function of the synthesis temperature (c). Color code: 300 $^{\circ}\text{C}$ (black), 400 $^{\circ}\text{C}$ (red), 500 $^{\circ}\text{C}$ (blue), 700 $^{\circ}\text{C}$ (green) and 800 $^{\circ}\text{C}$ (purple).

Chemical evolution of materials was further studied through XAES (**Figure S6**). From the first derivative of Auger CKLL peak the energy difference between the positive and negative maximum can be measured, which allows to calculate the D parameter (DP) value (**Table S2**). From this latter the sp^2/sp^3 ratio of carbons can be estimated,^[38,39] and amounts to 0.80, 0.83 and 0.87 for ZTC-300, -400 and -800, respectively. Similar information can be deduced from the C1s photoelectron peak position, which are centered at 284.78, 284.65 and 284.48 eV

for ZTC-300, -400 and -800, respectively (**Figure S7**). Pure graphene features a characteristic C1s peak at 284.40 eV (aromatic sp^2 carbon), whilst for graphene presenting structural defects and higher hydrogen content the peak shifts to higher binding energies.^[40] Hence, the shift to lower energies with growing synthesis temperature indicates decreasing sp^3 character of the sample. The evolution of C/O ratio observed from XPS is in agreement with what was deduced from elemental analysis, even if absolute values are higher in XPS (**Table S3**).

Functionalization of carbon materials with thiourea

Glycerol derived ZTCs were treated with thiourea with the aim to functionalize them with nitrogen and sulfur atoms. The textural properties are slightly impacted by the treatment and a reduction of the equivalent BET surface area and of the micropore volume of 5% was observed for all samples. No impact of the XRD long range order was observed upon functionalization. It appears that the oxygen content in the ZTCs plays a crucial role in the concentration of N and S atoms in functional materials (**Table S2**). Approximately 10at% and 4at% of N and S were detected by XPS, for ZTC-300-TU and ZTC-400-TU, which both feature a rather high amount of oxygen in the unfunctionalized samples (ZTC-300 and ZTC-400). By revenge, ZTC-800, which features a low amount of oxygen only permits for the functionalization with 2.6 and 1.8at.% of N and S, respectively. This hence indicates that N/S insertion requires the presence of oxygenated groups at the surface of the carbon backbone. Furthermore, after thiourea doping the C/O atomic ratio strongly decreases for all samples (**Table S3**). This could result from the substitution of some carbons with S and/or N atoms during the thermal treatment performed at 700 $^{\circ}\text{C}$ in the presence of thiourea.

To gather further information concerning the speciation of N and S atoms in thiourea-doped samples, XPS spectra of the S2p and N1s regions were recorded (**Figure 9a**). N1s spectra recorded with thiourea-doped ZTC materials were decomposed using four photopeaks, which are respectively assigned to pyridinic nitrogen (located at ca. 398.2 ± 0.1 eV), pyrrolic nitrogen (located at ca. 399.9 ± 0.1 eV), graphitic nitrogen (located at ca. 401.8 ± 0.5 eV) and oxidized nitrogen species (located at ca. 404.5 ± 0.5 eV).^[41] This latter contribution may be attributed to N atoms bonded with two C atoms and one O atom.^[42] From values reported in **Table S4**, it can be observed that the speciation of nitrogen only slightly depends on the ZTC synthesis temperature. For all materials, pyrrolic and pyridinic groups are mainly encountered. The main evolution concerns graphitic speciation with 7.8, 10.8 and 12.8at_N% for ZTC-300, ZTC-400 and ZTC-800, respectively. In addition, no covalent bond between nitrogen and sulfur atoms could be detected.

The high resolution spectrum of S2p region can be decomposed using multiple lines (**Figure 9b**). Two major peaks are located at ca. 163.9 and 165.1 eV, which represent the $\text{S}2p_{3/2}$ and $\text{S}2p_{1/2}$ doublet, with spin orbit splitting at ca. 1.2 eV. This doublet is associated with the presence of C-S like groups (C-S-C and C-S-H groups).^[43,44] The contribution at higher binding energy can be ascribed to the presence oxidized S atoms bounded to carbon atoms (-C-SO_n-). As described in **Table S5**, C-S-X (with X = C or H) functionalities are the most abundant speciation for sulfur atoms whatever the considered sample. It can be however noticed that for ZTC-800-TU a higher amount of C-S-X groups can be distinguished.

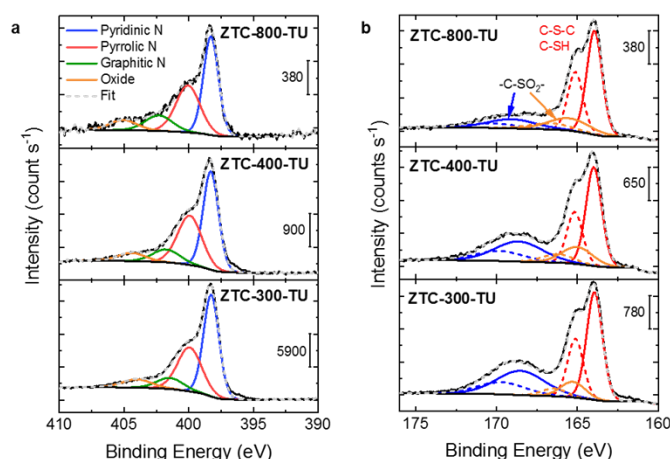


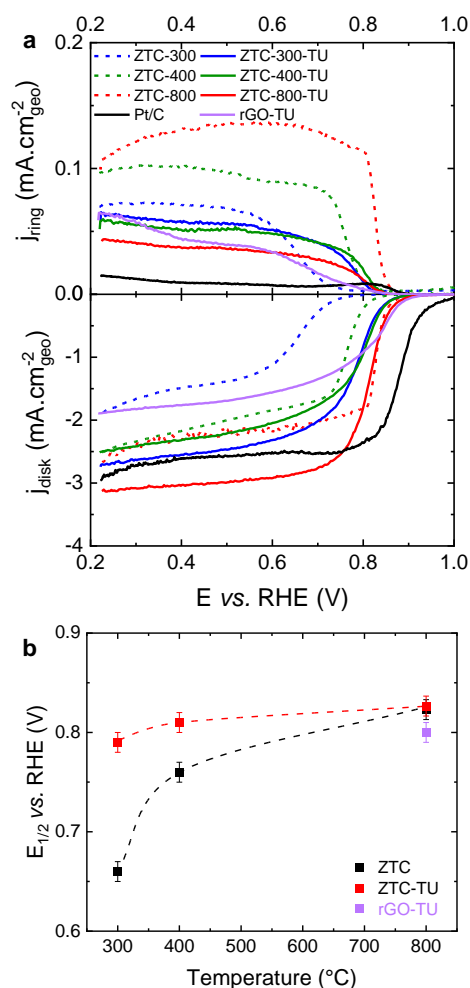
Figure 9. N1s (a) and S2p (b) XPS spectra of ZTC-300-TU, ZTC-400-TU, ZTC-800-TU.

Electrocatalytic tests

Polarization curves were recorded at 1600 rpm for each ZTC-based catalyst (**Figure 10**). Measurements with Pt/C and rGO-TU (*i.e.* reduced graphene oxide functionalized with thiourea in the same way as for the ZTCs) were realized as reference catalysts.

As far as the unfunctionalized ZTC samples are concerned, the synthesis temperature greatly affects the ORR activity (**Figure 10a**). The half wave potential increases from 0.66 to 0.82 V vs. RHE for ZTC-300 and ZTC-800, respectively (**Figure 10b**). Two different phenomena are responsible for the observed difference in activity. Firstly, the material synthesized at 300 °C (ZTC-300) is not fully condensed, which most probably affects the electrical conductivity of the material. In addition, ZTC-300 presents a low microporous volume ($0.65 \text{ cm}^3 \text{ g}^{-1}$), hence the active surface area is lower than for ZTC-400 for which a microporous volume of around $1 \text{ cm}^3 \text{ g}^{-1}$ was calculated. ZTC-800 material presents a rigid carbon skeleton mainly composed of sp^2 hybridized carbon atoms with high micropore volume. The sample moreover features turbostratic carbon on the external surface, which favors electrical conductivity.

The doping with thiourea improves the ORR activity of materials synthesized at 300 and 400 °C (ZTC-300-TU and ZTC-400-TU), (**Figure 10**). The interplay between nitrogen and sulfur atoms is known to allow for increasing the spin and charge densities of graphene networks, thus enabling a large number of carbon atoms to become active sites.^[45] The first synthesis step involves a heat treatment at 300 °C and 400 °C, respectively. During the second step, the doping with N and S atoms is performed at 750 °C. This step does not only engender the insertion of heteroatoms in the carbon backbone but also probably implies an increase in the graphitization degree of the carbon backbone. This is probably responsible for a higher electronic conductivity and thus for an improved charge transfer. This strongly enhances the reaction kinetics and thus the half-wave potential is shifted towards higher electrode potentials for ZTC-300-TU and ZTC-400-TU catalysts in comparison with ZTC-300 and ZTC-400 materials. For these two materials, the chemical composition, the amounts of sulphur and nitrogen atoms as well as their speciation are rather similar as shown by XPS measurements. For these two materials, half-wave potentials of 0.79 and 0.81 V vs. RHE were measured, which indicates that chemical functionalization allows to overcome low structural and textural quality in ZTC materials. The ORR activity of ZTC-800 is very similar to the one of ZTC-800-TU material (for both a half-wave potential of 0.82 V vs. RHE), probably in reason of the low amount of S and N atoms inserted in the carbon backbone (see XPS results). Moreover, the second step (enabling S and N



insertion in the carbon backbone) is performed at a temperature lower than 800 °C (*i.e.* 750 °C). The

Figure 10. a) RRDE polarization curves recorded with all ZTC-based catalysts and Pt/C reference catalyst. b) Half-wave potential measured on polarization curves recorded in Figure a. The half-wave potential obtained with rGO-TU catalyst is shown for comparison.

graphitization degree of the ZTC backbone is in this case is thus not affected by the second heat treatment. Thus the electronic conductivity of ZTC-800-TU and ZTC-800 samples must be close from each other. The activity of N,S functionalized ZTC materials is higher to that observed for the N,S-doped reduced graphene oxide sample (rGO-TU) and close to the activity of a reference Pt/catalyst (half-wave potential of 0.85 V vs. RHE). This catalyst is also one of the most efficient N and/or S-doped carbon-based catalysts reported to date (see **Table S6**). This highlights the interest in using ZTC-based catalysts as ORR catalysts, with respect to doped graphene-based samples, which suffer from sheet stacking.^[46,47] From RRDE experiments complementary information on the selectivity of the reduction process was obtained. The percentage of peroxide species formed during ORR as well as the number of electrons exchanged per oxygen molecule were determined from measured disk and ring currents (**Figure 11**). The hydroxyl selectivity of the reduction process is greatly improved after the insertion of nitrogen and sulfur atoms into the carbon backbone. For all N,S-doped ZTC catalysts, the amount of peroxide produced during the reduction process remains lower than 20%, and even below 12% for ZTC-800-TU in the whole potential range. This indicates that dual doping with nitrogen and sulfur

atoms plays a critical role in directing the oxygen reduction process toward the four-electron pathway.

Highest hydroxyl selectivity was observed for ZTC-800-TU, which might be associated to the higher number of graphitic N atoms (see XPS results). Finally, in this latter sample it is mostly probable that charge delocalization allows tuning the chemisorption mode of the O₂ molecule, favoring the side-on adsorption mode and thus facilitating the four-electron pathway.^[48] It is worth to note that the number of electrons exchanged per oxygen molecule and thus the hydroxyl selectivity of ORR is higher for ZTC-800-TU than for the graphene-based rGO-TU sample.

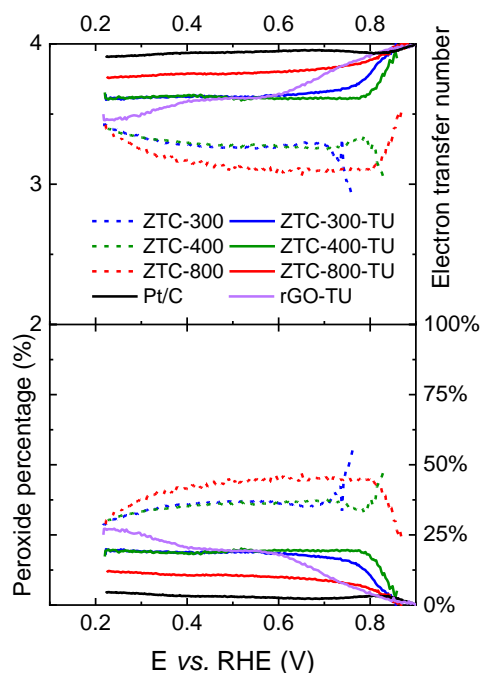


Figure 11. Number of electrons transferred per oxygen molecule (top) as well as fraction of peroxide formed during the reduction process (bottom). Calculations were done according to equations 2 and 3 using results shown in Figure 10a. Results obtained with Pt/C and rGO-TU materials are shown for comparison.

Conclusion

The synthesis of ZTCs using glycerol as carbon source was studied using synthesis temperatures from 300 to 800 °C. The textural and chemical properties were importantly impacted by the synthesis temperature. At 300 °C carbon materials without microporous long-range order were achieved featuring a flexible carbon network. At 400 °C high quality ZTCs featuring structured microporosity and high sp² carbon hybridization of the skeleton could be obtained. Materials synthesized at 800 °C present turbostratic carbon on the external surface of the ZTC. High ORR activity was observed even for unfunctionalized ZTC synthesized at 800 °C, yet with low selectivity towards the four-electron process. Nitrogen and sulfur functionalization of ZTCs was achieved through thiourea treatment. The amount of S and N functionalization was evidenced to depend on the oxygen content of the ZTC. ORR activities were substantially improved after functionalization even for the material synthesized at 300 °C. High quality N,S functionalized ZTCs derived from glycerol allowed for achieving superior ORR activity and hydroxyl selectivity in comparison to functional graphene-based materials. To complete this study, stability tests have to be performed and an in-depth analysis of structural changes affecting both the carbon backbone and the speciation of heteroatoms under working conditions should be performed.

Experimental Section

Materials

Glycerol (Sigma Aldrich, >99%), hydrofluoric acid (49% in water, Fisher Scientific), sodium bicarbonate (Sigma Aldrich, 99%), boric acid (Sigma Aldrich, 99%), nitrogen (99.995%, Air Liquide), thiourea (Sigma Aldrich, 99%) were purchased and used as received.

Synthesis of ZTC using glycerol

A similar reactor as previously described was used for the synthesis of ZTCs from glycerol.^[49] 1 g of the zeolite powder was introduced into a cylindrical quartz reactor containing a frit and activated at 150 °C for 1 hour under a nitrogen flow of 150 mL min⁻¹. The oven temperature was then raised to the target temperature (300 - 800 °C) and kept at this temperature for 1 hour. Glycerol feeding was started through a constant injection of 0.033 cm³ min⁻¹ to the nitrogen flow. After 4 h of feeding glycerol injection was ceased and the temperature was raised to 900 °C for 2 hours under nitrogen flow and then cooled down at room temperature. The recovered materials are named hybrid materials.

In order to remove the zeolite template 0.7 g of the hybrid materials was placed in a Teflon beaker and 7 mL of HF were added and kept under stirring for 4 h. Thereafter 42 mL of a saturated aqueous H₂BO₃ solution was added. The mixture was then neutralized through adding 42 mL of a saturated aqueous NaHCO₃ solution. After 1 hour of stirring at room temperature, the carbon materials was recovered by filtration using a polymer filter and washed using hot distilled water. After drying at 80 °C overnight, the final carbons were achieved. The samples were labelled ZTC-X where X corresponds to the synthesis temperature.

Thiourea treatment

The synthesis of N and S dual doped ZTC was performed by using thermally treated ZTC powders and thiourea as precursors. In a typical synthesis, 100 mg of ZTC powder was dispersed into 100 mL of ultrapure water. Then 1.6 g of thiourea are dissolved in the solution. The solution is homogenized by magnetic stirring for 30 minutes. Water is evaporated at 80 °C overnight before the powder is recovered and thermally treated at 700 °C for 2 h under a nitrogen flux (100 mL min⁻¹). The furnace is then cooled down at room temperature before the catalytic powder is recovered. The catalysts were labelled ZTC-X-TU where X corresponds to the synthesis temperature of ZTC material.

Characterization

The structural packing density (SPD) was determined via thermogravimetric analysis (TGA) using a SDT Q600 Waters device under air with a flow of 100 mL min⁻¹. Sample was heated to 900 °C with a ramp of 10 °C min⁻¹. The mean temperature of combustion was calculated from differential temperature analysis and corresponds to the value for which the differential temperature analysis signal reached a maximum. The SPD corresponds to the mass of carbonaceous species per gram of zeolite ($g_C g_{zeo}^{-1}$).^[25] Nitrogen physisorption isotherms were measured on a Micromeritics 3Flex at 77 K. Approximately 50 mg of sample were outgassed at 300 °C for 12 h before the measurement. Microporous volumes were calculated through the *t*-plot method. The thickness of the nitrogen layer was calculated using a reference isotherm of (i) non-porous silica (used for the *t*-plot of zeolites)^[50] and (ii) graphene (used for the *t*-plot of carbons).^[49] The apparent density of hybrid compounds (ρ_{App}) is a function of the SPD and of the occupied zeolite micropore volume and was calculated using Eq. (1) and is given as the ratio between the mass of carbonaceous species and its volume in the hybrid material ($g_C cm^3$).

$$\rho_{App} = \frac{SPD}{V_{micropore_i} - V_{micropore_f}} \quad (1)$$

where $V_{micropore_i}$ corresponds to the micropore volume of the zeolite template and $V_{micropore_f}$ to the micropore volume of the hybrid material. X-Ray powder diffraction (XRD) patterns were recorded on a PANalytical Empyrean X-Ray diffractometer using CuK α radiation (1.54059 Å) in the range of 5 - 50° 2 θ . Elemental analysis was performed using a Flash EA 1112/Flash 2000 Thermo instrument. Scanning Electron Microscopy (SEM) Transmission Electron Microscopy (TEM) was achieved on a JEOL JSM-790CF microscope and JEOL 2100 instrument, respectively. Raman spectra were obtained using 532 nm excitation wavelength on a LabRam HR 800-UV Horiba Jobin Yvon confocal microscope. XPS analyses were carried out with a Kratos Axis Ultra DLD spectrometer using a monochromatic Al K α source (1486.6 eV) operating at 180W (12 mA, 15 kV).

Electrochemical measurements

Electrochemical experiments were carried out using a home-made three electrodes Teflon cell at room temperature. A commercial hydrogen reference electrode (purchased by Gaskatel) and a glassy carbon slab were respectively used as reference and counter electrodes. The catalytic ink was performed by mixing 10 mg of catalytic powder, 750 μ L

of ultra-pure water, 250 μL of isopropanol and 100 μL of Nafion solution (5wt.% in a solution of aliphatic alcohols). The dispersion was finally dispersed by sonication to obtain a homogeneous solution. All experiments were carried out using a rotating ring disk electrode (Pine). All electrodes were connected to a biologic SP-300 potentiostat. The electrolyte was a 1 mol L^{-1} NaOH solution saturated with nitrogen or dioxygen. The working electrode was a glassy carbon disk (geometric surface area of 0.196 cm^2). For each experiment 7.5 μL of catalytic ink was deposited onto the glassy carbon disk and allowed to dry under nitrogen. Linear sweep voltammograms were recorded using the disk electrode at 1600 rpm by applying a scan rate of 5 mV s^{-1} to be under steady-state conditions. For all experiments the platinum ring was polarized at 1.2 V vs. RHE. The geometric surface of the ring is 0.11 cm^2 . From these experiments, the fraction of water formed ($p(\text{H}_2\text{O})$) as well as the number of electrons (n) exchanged per oxygen molecule during the reduction process can be calculated according to equations (2) and (3).^[51,52]

$$p(\text{H}_2\text{O}) = \frac{N|i_D| - |i_r|}{N|i_D| + |i_r|} \quad (2)$$

$$n = 4p(\text{H}_2\text{O}) + 2(1 - p(\text{H}_2\text{O})) \quad (3)$$

Where N is the collection efficiency (21.8%), i_D and i_r correspond to the intensities measured with disk and ring currents, respectively.

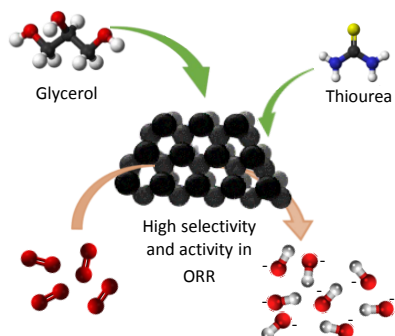
Acknowledgements

Authors acknowledge financial support from the European Union (ERDF) and "Région Nouvelle Aquitaine" and from the CAPES-COFEUCB program (#88881.370977/2019-01 and #45020TE). The authors acknowledge the European Union (ERDF) and Région Nouvelle Aquitaine for the funding of MABATRI and PLATABAT projects (reference 2021-16148810 and reference 2022- 23222510).

Keywords: Zeolite-templated carbons • Glycerol • Carbon • ORR • Graphene

- [1] T. Zhang, C. Liu, Y. Gu, F. Jérôme, *Green Chem.* **2021**, *23*, 7865-7889.
- [2] M. Checa, S. Nogales-Delgado, V. Montes, J. M. Encinar, *Catalysts* **2020**, *10*, 1279.
- [3] Y. Wang, M. Zhang, X. Shen, H. Wang, H. Wang, K. Xia, Z. Yin, Y. Zhang, *Small* **2021**, *17*, 2008079.
- [4] S. Mehta, S. Jha, H. Liang, *Renewable Sustainable Energy Rev.* **2020**, *134*, 110345.
- [5] A. Celzard, V. Fierro, *Carbon* **2020**, *167*, 792-815.
- [6] R. S. Ribeiro, A. M. Silva, M. T. Pinho, J. L. Figueiredo, J. L. Faria, H. T. Gomes, *Catal. Today*, **2015**, *240*, 61-66.
- [7] M. d. A. Medeiros, T. M. Cançado, C. M. M. Leite and R. M. Lago, *J. Chem. Technol. Biotechnol.* **2012**, *87*, 1654-1660.
- [8] Y. Cui, John D. Atkinson, *J. Mater. Chem. A* **2017**, *5*, 16812-16821.
- [9] M. Gonçalves, C. S. Castro, I. K.V. Boas, F. C. Soler, E. de C. Pinto, R. L. Lavall, W. A. Carvalho, *J. Environ. Chem. Eng.* **2019**, *7*, 103059.
- [10] A. Celzard, V. Fierro, J. F. Mareche, G. Furdin, *Adsorpt. Sci. Technol.* **2007**, *25*, 129-142.
- [11] Z. Ma, T. Kyotani, A. Tomita, *Chem. Commun.*, **2000**, 2365–2366.
- [12] K. Matsuoka, Y. Yamagishi, T. Yamazaki, N. Setoyama, A. Tomita, T. Kyotani, *Carbon*, **2005**, *43*, 855–894.
- [13] P.X. Hou, T. Yamazaki, H. Orikasa, T. Kyotani, *Carbon*, **2005**, *43*, 2618–2641.
- [14] K. Kim, T. Lee, Y. Kwon, Y. Seo, J. Song, J. Ki Park, H. Lee, J. Young Park, H. Ihee, S. June Cho, R. Ryoo, *Nature* **2016**, *353*, 131-135.
- [15] H. Nishihara, Q.H. Yang, P.X. Hou, M. Unno, S. Yamauchi, R. Saito, J. I. Paredes, A. Martínez-Alonso, J. M.D. Tascon, Y. Sato, M. Terauchi, T. Kyotani, *Carbon*, **2009**, *47*, 1220-1230.
- [16] F. Su, J. Zeng, Y. Yu, L. Lv, J. Y. Lee, X.S. Zhao, *Carbon*, **2005**, *43*, 2366–2373.
- [17] H. Nishihara, P.X. Hou, L.X. Li, M. Ito, M. Uchiyama, T. Kaburagi, A. Ikura, J. Katamura, T. Kawarada, K. Mizuuchi, T. Kyotani, *J. Phys. Chem. C*, **2009**, *113*, 3189–3196.
- [18] H. Itoi, H. Nishihara, T. Kogure, T. Kyotani, *J. Am. Chem. Soc.*, **2011**, *133*, 1165–1167.
- [19] J. Wang, Z. Liu, X. Dong, C.E. Hsiung, Y. Zhu, L. Liua, Y. Han, *J. Mater. Chem. A*, **2017**, *5*, 6860-6865.
- [20] H. Nishihara, T. Kyotani, *Chem. Commun.* **2018**, *54*, 5648-5673.
- [21] R. Ruiz-Rosas, M. J. Valero-Romero, D. Salinas-Torres, J. Rodríguez-Mirasol, T. Cordero, E. Morallón, D. Cazorla-Amorós, *ChemSusChem*, **2014**, *7*, 1458-1467.
- [22] H. Itoi, C. Matsuoka, R. Hirade, G. Saeki, S. Sugiyama, K. Morishita, Y. Kasai, H. Iwata, Y. Ohzawa, *Carbon Trends*, **2022**, *9*, 100228.
- [23] H. Park, J. Bang, S. Won Han, R. Kumar Bera, K. Kim, R. Ryoo, *Microporous Mesoporous Mater.*, **2021**, *318*, 111038.
- [24] E. E. Taylor, K. Garman, N. P. Stadie, *Chem. Mater.*, **2020**, *32*, 2742–2752.
- [25] T. Aumond, I. Batonneau-Gener, Y. Pouilloux, L. Pinard, D. Wisser, M. Moreau, H. Vezin, A. Moissette, A. Sachse, *Mater. Today Chem.* **2022**, *26*, 101053.
- [26] J. Weber, J. Schmidt, A. Thomas, W. Böhlmann, *Langmuir* **2010**, *26*, 15650-15656.
- [27] N. P. Stadie, J. J. Vajo, R. W. Cumberland, A. A. Wilosn, C. C. Ahn, B. Fultz, *Langmuir* **2012**, *28*, 10057-10063.
- [28] P. Toth, *Carbon*, **2021**, *178*, 688-707.
- [29] M. Shtein, I. Pri-Bar, M. Varenik, O. Regev, *Anal. Chem.* **2015**, *87*, 4076–4080.
- [30] B. Dou, V. Dupont, P. T. Williams, H. Chen, Y. Ding, *Bioresour. Technol.* **2009**, *100*, 2613-2620.
- [31] T. Valliyappan, N.N. Bakhshi, A.K. Dalai, *Bioresour. Technol.* **2008**, *99*, 4476-4483.
- [32] M. W. Smith, I. Dallmeyer, T. J. Johnson, C. S. Brauer, J.-S. McEwen, J. F. Esoinal, M. Garcia-Perez, *Carbon*, **2016**, *100*, 678-692.
- [33] J. Schwan, S. Ulrich, V. Batori, H. Ehrhardt, *J. Appl. Phys.* **1996**, *80*, 440-447.
- [34] K. H. Michaelian, S. A. Oladepo, J. M. Shaw, X. Liu, D. Bégué, I. Baraille, *Vib. Spectrosc.* **2014**, *74*, 33-46.
- [35] A. C. Ferrari, *Solid State Commun.* **2007**, *143*, 47-57.
- [36] F. Negri, C. Castiglioni, M. Tommasini, G. Zerbi, *J. Phys. Chem. A* **2002**, *106*, 3306-3317.
- [37] M. Rigolio, C. Castiglioni, G. Zerbi, F. Negri, *J. Mol. Struct.* **2001**, *563*-364, 79-87.
- [38] J.C. Lascovich, S. Scagkione, *Appl. Surf. Sci.* **1994**, *78*, 17-23.
- [39] L. Calliari, *Diamond Relat. Mater.* **2005**, *14*, 1232-1240.
- [40] D. J. Morgan, *Journal of Carbon Research*, **2021**, *7*, 51-59
- [41] T. Susi, T. Pichler, P. Ayala, *Beilstein J. Nanotechnol.* **2015**, *6*, 177-192.
- [42] G. Hasegawa, T. Deguchi, K. Kanamori, Y. Kobayashi, H. Kageyama, T. Abe, K. Nakanishi, *Chem. Mater.* **2015**, *27*, 4703-4712.
- [43] X. Yu, H. S. Park, *Carbon* **2014**, *77*, 59-65.
- [44] D. Saha, S. Barakat, S. E. Van Bramer, K. A. Nelson, D. K. Hensley, J. Chen, *ACS Appl. Mater. Interfaces* **2016**, *8*, 34132–34142.
- [45] W. Chen, X. Chen, R. Qiao, Z. Jiang, Z.-J. Jiang, S. Papović, K. Raleva, D. Zhou, *Carbon*, **2022**, *187*, 230-240.
- [46] T. Aumond, V. Fogiel, L. Leandro dos Santos, I. Batonneau-Gener, Y. Pouilloux, C. Comminges, C. Canaff, S. B.C. Pergher, A. Habrioux, A. Sachse, *Mol. Catal.*, **2022**, *531*, 112669.
- [47] J. Wang, G. Wang, S. Miao, J. Liab, X. Bao, *Faraday Discuss.*, **2014**, *176*, 135-151.
- [48] Z. Shi, J. Zhang, Z.- Liu, H. Wang, D. P. Wilkinson, *Electrochim. Acta*, **2006**, *51*, 1905–1916.
- [49] T. Aumond, J. Rousseau, Y. Pouilloux, L. Pinard, A. Sachse, *Carbon Trends*, **2021**, *2*, 100014.
- [50] I. Batonneau-Gener, A. Sachse, *J. Phys. Chem. C*, **2019**, *123*, 4235-4242.
- [51] A. Habrioux, D. Diabaté, J. Rousseau, T. W. Napporn, K. Servat, L. Guétaz, A. Trokourey, K. B. Kokoh, *Electrocatalysis*, **2010**, *1*, 51–59.
- [52] F. T. A. Vork, E. Barendrecht, *Electrochim Acta*, **1990**, *35*, 135-139.

Entry for the Table of Contents



Bio-sourced synthesis of Zeolite-Templated Carbons (ZTCs) was achieved through the use of glycerol as carbon source. Oxygen content depends on synthesis temperature and importantly impacts the post-synthetic functionalization with N and S atoms. N,S-functionalized ZTCs allow for achieving conspicuous activities and selectivity towards the four-electron process.